Journal of Nuclear Materials 386–388 (2009) 143–146

Contents lists available at ScienceDirect

Journal of Nuclear Materials

journal homepage: www.elsevier.com/locate/jnucmat

Irradiation creep and microstructural changes in an advanced ODS ferritic steel during helium implantation under stress

J. Chen [a,*], M.A. Pouchon [a], A. Kimura [b], P. Jung [c], W. Hoffelner [a]

[a] Department of Nuclear Energy and Safety, Paul Scherrer Institute, CH-5232 Villigen-PSI, Switzerland
[b] Institute of Advanced Energy, Kyoto University, Gokasho, Uji, Kyoto 611-0011, Japan
[c] Institute für Festkörperforschung, Forschungszentrum Jülich, D-52425 Jülich, Germany

A B S T R A C T

An advanced oxide dispersion strengthened (ODS) ferritic steel with very fine oxide particles has been homogeneously implanted with helium under uniaxial tensile stresses from 20 to 250 MPa to a maximum dose of about 0.38 dpa (1650 appm-He) with displacement damage rates of 4.4×10^{-6} dpa/s at temperatures of 573 and 773 K. The samples were in the form of miniaturized dog-bones, where during the helium implantation the straining and the electrical resistance were monitored simultaneously. Creep compliances were measured to be 4.0×10^{-6} and 11×10^{-6} dpa^{-1} MPa^{-1} at 573 and 773 K, respectively. The resistivity of ODS steel samples decreased with dose, indicating segregation and/or precipitation. Evolution of microstructure during helium implantation was studied in detail by TEM. The effects of ODS particle size on irradiation creep and microstructural changes was investigated by comparing the results from the present advanced ODS (K1) to a commercial ODS ferritic steels (PM2000) with much bigger oxide particles.

1. Introduction

Their superior high-temperature properties and high potential in resistance to irradiation and corrosion, have stimulated worldwide investigations on oxide dispersion strengthened (ODS) ferritic/martensitic steels for application in advanced nuclear energy systems, such as fusion reactors and generation IV fission reactors in the last decade [1–6]. For instance, the application of ODS steels to blanket components in a fusion reactor will increase thermal efficiency and provide a larger design tolerance. To use ODS steels in nuclear energy systems, many efforts have been made to optimise production processes and to characterise their mechanical and corrosion properties [1–6]. On the other hand, studies on irradiation effects in general are still very limited and especially irradiation creep data are almost completely missing. Recently, irradiation creep [7] and related microstructural changes [8] of an industrially produced ODS steel (PM2000) [9] have been reported. As advanced 19Cr ODS steels, for example the newly developed type K1 of Kyoto University have much smaller ODS particles, it was the aim of the present work to investigate the effects of oxide particle size on irradiation creep and microstructural changes under irradiation. Therefore, in the present work, in-situ irradiation creep of the advanced 19Cr ODS steel K1, and resistivity changes were investigated. Irradiation was performed by homogeneous implantation of helium ions. During irradiation, tensile strain measurement was performed to monitor irradiation creep, while simultaneous resistivity measurements gave gross indications of microstructural changes. Detailed investigations of microstructural changes were obtained from transmission electron microscopy (TEM) after implantation.

2. Experimental

The advanced ODS ferritic alloy developed in Kyoto University was in a rod bar (ϕ23 mm) form with the composition (wt%, balance Fe) 0.05% C, 0.041% Si, 0.06% Mn, 18.37% Cr, 0.29% W, 0.28% Ti, 0.014% N and 0.368% Y_2O_3. The detailed production process has been described in Refs. [1,5,6]. TEM observation show that the as-received alloy has nano-sized grains with quite uniformly distributed ODS particle. The dislocation density shows significant grain-to-grain variations. Examples of TEM micrographs are given in Fig. 1, showing grain shape and size (a), dislocation network (b) and ODS particle distribution (c), respectively. In the as-received condition the grains with sizes of roughly $200 \times 200 \times 700$ nm^3 are elongated along the rolling direction. The average diameter of the ODS particles is 2.1 ± 0.5 nm and their number density is estimated to $1.2 \times 10^{24}/m^3$. Dog-bone shaped creep specimens of 300 μm thickness were cut by spark erosion parallel to the rolling direction. The samples were mechanical polished on both sides to 100 μm with grad 2400 paper. The final samples had

* Corresponding author. Tel.: +41 56 310 2280; fax: +41 56 310 4595.
E-mail address: jiachao.chen@psi.ch (J. Chen).

0022-3115/$ - see front matter © 2008 Elsevier B.V. All rights reserved.
doi:10.1016/j.jnucmat.2008.12.081

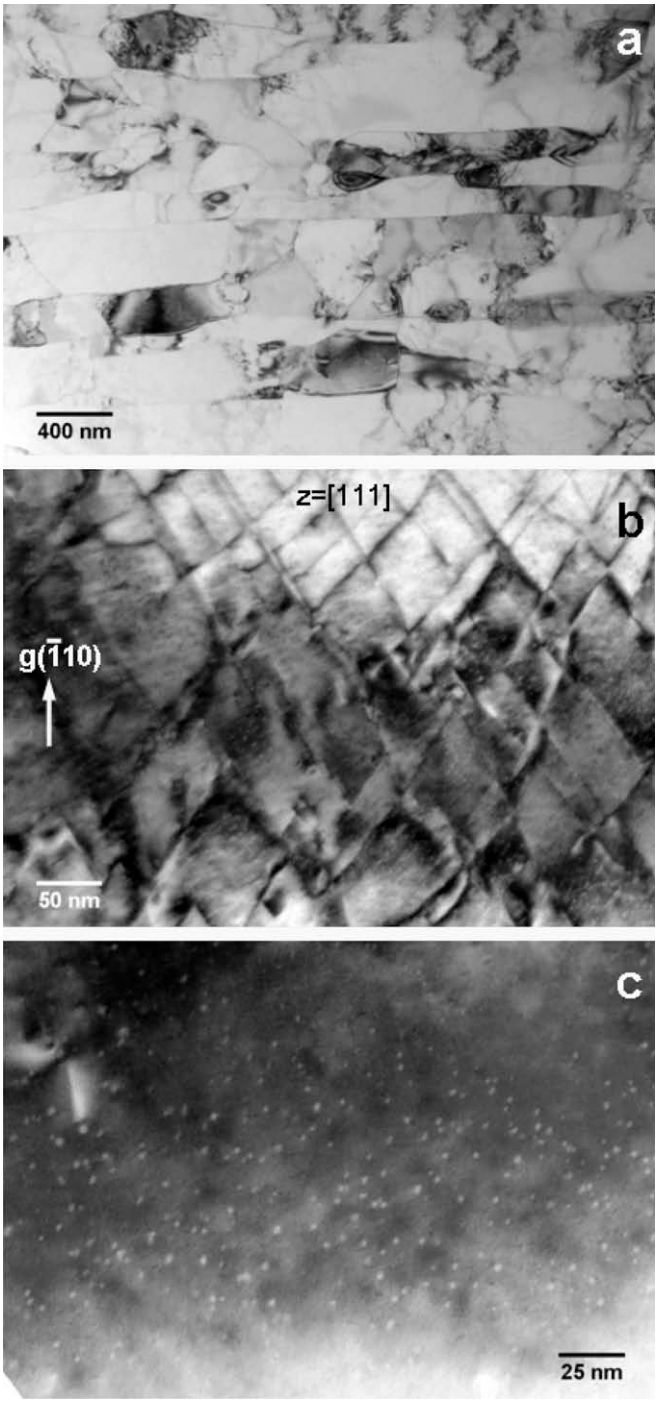

Fig. 1. Microstructure of as received 19Cr ODS steel (K1) showing the shape and size of grains (a), the dislocation network (b) and the ODS particle distribution (c).

an overall size of 28 mm in length, 8 mm in width and 0.1 mm in thickness, with a gauge volume of $10 \times 2 \times 0.1$ mm^3.

In-situ creep under He-implantation was performed at the Compact Cyclotron of Forschungszentrum Juelich. Details of the experimental set up are described in Ref. [10]. The gauge area of the 0.1 mm thick samples was 3D-homogeneously implanted under constant uniaxial stress [9,10]. Typical implantation rates were 0.019 appm-He per second. The concurrent production of displacement damage was calculated by TRIM and SRIM for a displacement threshold energy of 40 eV and a binding energy of 3 eV, giving per implanted He-atom 275 displacements on the front side and 193

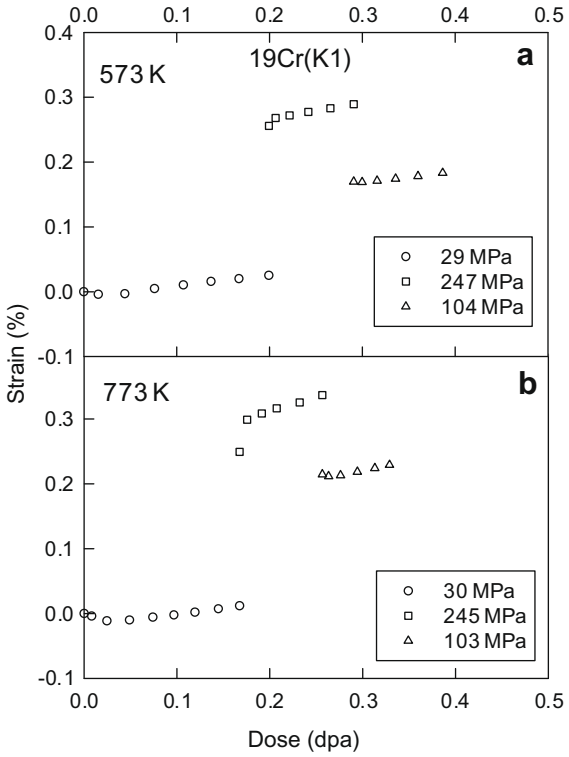

Fig. 2. Strain of 19Cr ODS steel (K1) during He-implantation at 573 (a) and 773 K (b) as a function of displacement dose at different stresses.

on the back side, averaging to 234 displaced lattice atoms. With an average beam current density of 5.0 μA/cm^2, a displacement rate of about 4.4×10^{-6} dpa/s (displacements per atom per second) is derived. The irradiation creep strains were monitored by LVDT (Linear Variable Displacement Transducer) while the resistance was derived by a four-pole technique during beam-off periods. The implantation was continued until the strain rate became constant (stationary creep). Then, implantation of the same specimen was resumed at a different stress in the range of 20–250 MPa. To minimize systematic errors from dose effects on the microstructure, e.g. by accumulation of irradiation defects, applied stress was changed alternatively to higher and lower values as indicated in Fig. 2. For each specimen, the temperature was fixed at 573 or 773 K, respectively. The temperature distribution along the gauge region was monitored by an infrared pyrometer under 45° from the backside of the specimens. Finally, TEM specimens were prepared from the implanted gauge sections (see Ref. [11] for details) and TEM examinations were performed with a JEM 2010 at PSI.

3. Results and discussion

3.1. Irradiation creep

Fig. 2 shows the strain $\varepsilon(\sigma) = \frac{\Delta l}{l_0}$ of 19Cr ODS steel (K1) during implantation as a function of the displacement dose at 573 (a) and 773 K (b), respectively. At both temperatures, a contraction of the specimen against the applied tensile stress occurs at the beginning of irradiation, but already after 0.05 dpa, creep in the stress direction prevails. Each stress change caused, aside from elastic strain, also a short transient stage before stationary creep was reached again. Those transient strains are similar to observations in PM2000 [7] and are ascribed to irradiation-induced relaxation. According to the results from PM2000 [7], it is assumed that thermal creep is negligible even at 773 K. Irradiation-induced

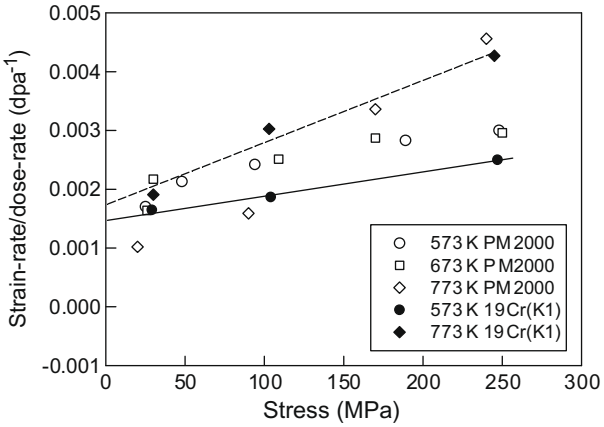

Fig. 3. Irradiation creep rates per displacement rates of 19Cr ODS steel (K1) as a function of tensile stress under He-implantation at 573 and 773 K. From linear fits irradiation creep compliances are derived. The PM2000 data [9] are included for comparison.

creep rates, ε' i.e. strain-rate per dose-rate (in unit of dpa^{-1}) were obtained by fitting straight lines to the stationary parts of the curves in Fig. 2. These values are plotted in Fig. 3 as a function of the applied stress for both implantation temperatures. The data from PM2000 are also included for comparison. The data can be fitted by linear stress dependences up to 250 MPa:

$$\varepsilon'(\sigma) = B_0 \cdot \sigma + \varepsilon'_0 \quad (1)$$

with creep compliances B_0, i.e. creep rate per dose rate (assuming linear dependence) and stress, of 4.0×10^{-6} and 11×10^{-6} dpa^{-1} MPa^{-1} at temperatures of 573 K (solid line) and 773 K (dashed line), respectively. Extrapolating the lines in Fig. 3 to zero stress gives ordinate-offsets ε'_0 of 1.50×10^{-3} and 1.72×10^{-3} dpa^{-1} at temperatures of 573 and 773 K, respectively. ε'_0 represents stress-independent dimensional changes, for example from volume swelling:

$$\frac{\Delta V}{V} = 3 \cdot \varepsilon'_0. \quad (2)$$

The irradiation creep compliance at 573 K of the present steel is almost identical to that of PM2000 at temperatures $\leqslant$673 K. At 773 K creep compliance increases, but to a little lesser extent, compared to PM2000. This means that ODS particle size does not influence significantly the irradiation creep properties.

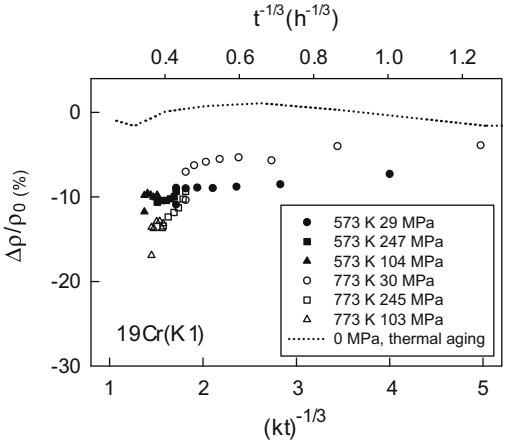

Fig. 4. Relative changes of electrical resistivity (measured at room temperature) of 19Cr ODS steel (K1) during He-implantation at 573 and 773 K at indicated stresses. The dotted line refers to thermal aging without stress at 773 K.

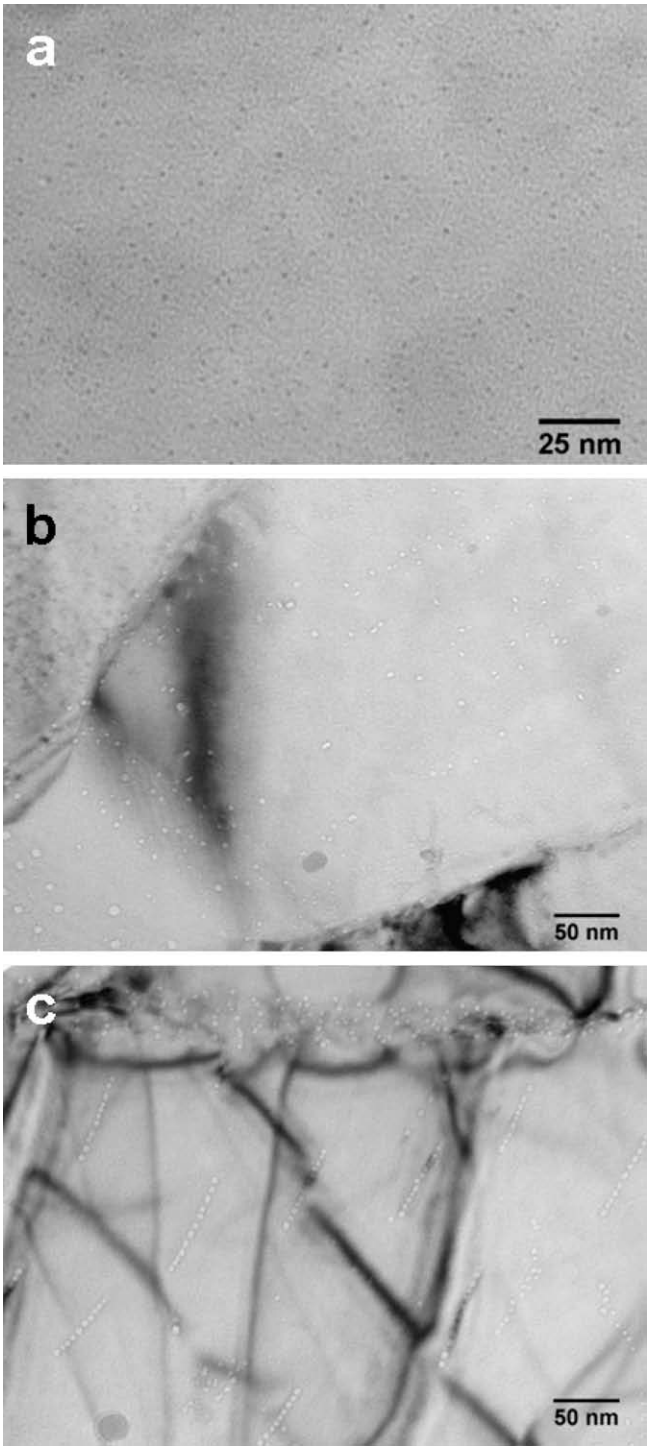

Fig. 5. Over- (a) and under-focused (b, c) bright-field images showing the bubble distribution after implantation of 1650 appm-He at 573 K and 1400 appm-He at 773 K, respectively. Notice that the bubble distribution at 773 K (b, c) shows strong grain-to-grain variations.

3.2. Resistivity

During irradiation resistance measurements were performed after switching off the α-beam and waiting for 12 min to stabilise temperature near ambient. As these measurements were performed under various stresses, effects of elastic strains on specimen geometry have to be considered. Using resistance-stress relations measured before irradiation, assuming that irradiation

does not change these relations, gave corrections of less than 0.3% which therefore were neglected. Thermal aging experiments were performed under 0 MPa at 773 K and resistance was measured at room temperature. This measurement showed very small increase of resistivity, while a significant decrease of resistivity is observed under implantation/irradiation. In Fig. 4, the evolution of electrical resistivity during irradiation (symbols) and thermal aging (dashed line) is compared. The electrical resistivity data are plotted for a $(kt)^{-1/3}$ dose dependence (k is damage rate, t is time) in the case of irradiation and for a $t^{-1/3}$ in the case of thermal aging. Such dependence would be expected for diffusion controlled growth of precipitates [12–14]. The results in Fig. 4 conform to a $(kt)^{-1/3}$ behaviour at 573 K but suggests a two-stage process at 773 K with a strong decrease at longer times. This is tentatively ascribed to decomposition of Fe-Cr solution during the first stage ($kt^{-1/3} > 2$) followed by the formation of Cr-rich α' precipitates (at $kt^{-1/3} < 2$) [15]. The resistivity changes of K1 in Fig. 4 at 557 K as well as 773 K are quite similar to those obtained for PM2000 [7].

3.3. TEM observation

TEM was conducted after in-situ creep test. The complex dislocation structure of the as-received material prevents discrimination of minor changes. In other word, no remarkable change of the dislocation structure could be detected. However, bubbles formed during implantation at both temperatures. Fig. 5 shows an over-focused bright field image of a sample irradiation creep tested at 573 K (a), and an under-focused bright field image of a sample irradiation creep tested at 773 K (b,c). The Gaussian distributed helium bubbles have an average size of 1.1 ± 0.2 nm and a number density of roughly 1×10^{23} m^{-3} at 573 K, while at 773 K bubble features change from grain to grain (Fig. 5(b)), showing sizes from 2 to 7 nm and shapes from spherical to facetted. Fig. 5(c) shows bubbles arranged on lines, resulting from an edge-on view of disk shaped bubble-loop complexes [8]. Compared to the PM2000 steel [7], K1 features smaller size and lower density of bubbles and much lower dislocation density. This suggests superior resistance of this 19Cr ODS steel against helium embrittlement.

4. Summary and conclusion

The irradiation creep, resistivity and microstructural change of an advanced 19Cr ODS steel has been investigated and the main results can be summarized as following:

(1) Irradiation creep rates of 19Cr ODS steel show linear stress dependence up to 250 MPa at temperatures from 573 to 773 K.
(2) Irradiation creep rate per dose rate and stress amounts to 4.0×10^{-6} and 11×10^{-6} dpa^{-1} MPa^{-1} at temperatures of 573 and 773 K, respectively. No remarkable effects of ODS particle size on irradiation creep properties is observed.
(3) The resistivity of 19Cr ODS decreases with increasing displacement dose, indicating segregation and/or precipitation.
(4) Suppression of growth of helium bubbles by fine ODS particles may increase the resistance of 19Cr ODS ferritic steels against helium embrittlement.

According to above results one can conclude that:

(1) Irradiation creep of ODS steels is not significantly affected by the size of the dispersed oxides
(2) Smaller and denser ODS particle give less growth of helium bubbles which may cause higher resistance against helium embrittlement.

Acknowledgements

The authors are grateful to H. Klein, L. Kasterke, and B. Olefs of FZ Juelich for operation of the cyclotron. Work was performed within the Swiss Generation IV Program. It was partially financed by EU-projects EXTREMAT and RAPHAEL.

References

[1] Akihiko Kimura, Mater. Trans. 46 (2005) 394.
[2] A. Alamo, H. Regle, G. Pons, L.L. Bechade, Mater. Sci. Forum 88&90 (1992) 183.
[3] M. Klimiankou, R. Lindau, A. Moeslang, J. Schroeder, Powder Metall. 48 (2005) 277.
[4] A. Ramar, Z. Oksiuta, N. Baluc, R. Schäublin, Fus. Eng. Des. 82 (2007) 2543.
[5] S. Ukai, M. Fujiwara, J. Nucl. Mater. 307&311 (2002) 749.
[6] N.Y. Iwata, A. Kimura, M. Fujiwara, N. Kawashima, J. Nucl. Mater. 367&370 (2007) 191.
[7] J. Chen, P. Jung, M.A. Pouchon, T. Rebac, W. Hoffelner, J. Nucl. Mater. 373 (2008) 22.
[8] J. Chen, P. Jung, W. Hoffelner, H. Ullmaier, Acta Mater. 56 (2008) 250.
[9] Dispersion-Strengthened High-Temperature Materials, Material Properties and Applications, Prospectus from Plansee (2003), 706 DE.04.03(1000)RWF.
[10] P. Jung, A. Schwarz, H.K. Sahu, Nucl. Instrum. and Meth. A234 (1985) 331.
[11] J. Chen, P. Jung, M. Nazmy, W. Hoffelner, J. Nucl. Mater. 352 (2006) 36.
[12] K. Binder, D. Stauffer, Z. Physik. B24 (1976) 407.
[13] I.M. Lifshitz, V.V. Slyozov, J. Phys. Chem. Sol. 19 (1961) 35.
[14] C. Wagner, Z. Elektrochemie 65 (1961) 581.
[15] H.S. Cho, R. Kasada, A. Kimura, J. Nucl. Mater. 367&370 (2007) 239.